AIAA JOURNAL
Vol. 45, No. 10, October 2007

Dynamic Snap-Through of Thin-Walled Structures by a Reduced-Order Method

Adam Przekop*
National Institute of Aerospace, Hampton, Virginia 23666
and
Stephen A. Rizzi†
NASA Langley Research Center, Hampton, Virginia 23681

DOI: 10.2514/1.26351

The goal of this investigation is to further develop nonlinear modal numerical simulation methods for application to geometrically nonlinear response of structures exposed to combined high-intensity random pressure fluctuations and thermal loadings. The study is conducted on a flat aluminum beam, which permits a comparison of results obtained by a reduced-order analysis with those obtained from a numerically intensive simulation in physical degrees of freedom. A uniformly distributed thermal loading is first applied to investigate the dynamic instability associated with thermal buckling. A uniformly distributed random loading is added to investigate the combined thermal-acoustic response. In the latter case, three types of response characteristics are considered, namely: 1) small-amplitude vibration around one of the two stable buckling equilibrium positions, 2) intermittent snap-through response between the two equilibrium positions, and 3) persistent snap-through response between the two equilibrium positions. For the reduced-order analysis, four categories of modal basis functions are identified, including those having symmetric transverse, antisymmetric transverse, symmetric in-plane, and antisymmetric in-plane displacements. The effect of basis selection on the quality of results is investigated. It is found that despite symmetric geometry, loading, and boundary conditions, the antisymmetric transverse and symmetric in-plane modes participate in the snap-through behavior.

Nomenclature

$\boldsymbol{C}, \tilde{\boldsymbol{C}}$	=	proportional damping matrix (physical and modal coordinates)
d, a, b	=	linear, quadratic nonlinear, and cubic nonlinear modal stiffness coefficients
$\boldsymbol{F}, \tilde{\boldsymbol{F}}$	=	force excitation vector (physical and modal coordinates)
$\boldsymbol{F}_{NL}, \tilde{\boldsymbol{F}}_{NL}$	=	nonlinear restoring force (physical and modal coordinates)
$[\boldsymbol{I}]$	=	identity matrix
$\boldsymbol{K}, \tilde{\boldsymbol{K}}$	=	stiffness matrix (physical and modal coordinates)
$\boldsymbol{M}, \tilde{\boldsymbol{M}}$	=	mass matrix (physical and modal coordinates)
t	=	time
u, v, ϕ	=	horizontal and vertical displacement, and rotation (global physical coordinates)
$\boldsymbol{X}, \boldsymbol{q}$	=	displacement response vector (physical and modal coordinates)
α	=	thermal expansion coefficient
ΔT	=	temperature increment
ζ	=	viscous damping factor
$\boldsymbol{\Phi}$	=	modal basis function matrix
ω	=	undamped natural frequencies

Presented as Paper 1745 at the 47th AIAA/ASME/ASCE/AHS/ASC Structures, Structural Dynamics & Materials Conference, Newport, RI, 1–4 May 2006; received 13 July 2006; revision received 11 April 2007; accepted for publication 5 May 2007.

*Research Scientist. Senior Member AIAA.
†Aerospace Engineer, Structural Acoustics Branch. Associate Fellow AIAA.

I. Introduction

DIRECT numerical simulation of nonlinear random response in physical degrees of freedom (DOF) is computationally intensive even for the simplest structures. Its use for design of high-cycle-fatigue-tolerant aerospace vehicle structures, requiring long simulation times to obtain meaningful statistics, is considered impractical. Accordingly, much effort has been spent in recent years to develop accurate reduced-order analyses such as finite-element-based nonlinear modal numerical simulation, which could be suitable for use in design environments.

Aerospace structures exposed to a high-intensity random acoustic loading are often also simultaneously exposed to an elevated thermal environment [1]. Because both acoustic and thermal loadings can cause the structure to respond in a geometrically nonlinear fashion, an analysis technique that permits simultaneous loading is required (i.e., linear superposition of the acoustic and thermal response is not suitable). Under certain thermal-acoustic loading conditions, experimental studies indicate a snap-though response [2–4], which can significantly reduce fatigue life. The snap-through problem has previously been investigated using reduced-order analyses with both closed-form [5–11] and finite element (FE) [12–15] solutions. Reduced-order FE analysis can be further classified into so-called direct [12–14] and indirect [15] stiffness evaluation procedure approaches. For both direct and indirect approaches, the system is first transformed to a reduced set of coupled nonlinear equations, which are solved via numerical integration. Because the eventual application is the analysis and design of practical structures, this paper focuses on developments associated with the indirect approach, which has been implemented for use with commercial finite element codes [15–17]. The previous work [15] using the indirect procedure modeled the dynamic snap-through response with a single transverse mode. However, it has been subsequently shown that a significant improvement can be obtained using a basis consisting of both low-frequency transverse-dominated modes and high-frequency in-plane-dominated modes [17,18]. The present work concentrates on selecting such a basis so that both the transverse and in-plane dynamic behaviors of the system can be accurately modeled.

A clamped–clamped aluminum beam is considered in this work to allow reduced-order analysis results to be compared with a numerically intensive simulation in physical DOF. The dynamic thermal-buckling problem is first studied by applying a uniformly distributed positive temperature increment. The combined thermal-acoustic loading is subsequently investigated through the addition of uniformly distributed acoustic loadings of different intensities. Several response characteristics are investigated, including 1) small-amplitude vibration around one of two stable buckled equilibrium positions, 2) intermittent snap-through response between the two buckled equilibrium positions, and 3) persistent snap-through response between the two buckled equilibrium positions. In each case, the reduced-order analysis is performed with two different sets of basis functions, and results are compared with those obtained by numerical simulation in physical DOF.

II. Reduced-Order Numerical Simulation

The reduced-order analysis is first presented, because it is used to study the response to both thermal and thermal-acoustic loadings. Similarities between the direct and indirect stiffness evaluation methods are discussed.

A. Modal Coordinate Transformation

In the direct stiffness evaluation approach, the equations of motion for a nonlinear system subjected to a change in temperature can be expressed in the form [12–14]

$$\boldsymbol{M}\ddot{\boldsymbol{X}}(t) + \boldsymbol{C}\dot{\boldsymbol{X}}(t) + \{K_L - K_{\Delta T}(\Delta T) + K_1[\boldsymbol{X}(t)] + K_2[\boldsymbol{X}(t), \boldsymbol{X}(t)]\}\boldsymbol{X}(t) = \boldsymbol{F}(t) + \boldsymbol{F}_{\Delta T} \tag{1}$$

where $\boldsymbol{M}$ is the mass matrix; $\boldsymbol{C}$ is the mass proportional damping matrix (no temperature dependence is assumed); K_L, K_1, and K_2 are the linear, quadratic, and cubic stiffness matrices, respectively; $\boldsymbol{X}$ is the displacement response vector; and $\boldsymbol{F}$ is the force excitation vector. The thermal effect is present on both sides of Eq. (1): as a change in the linear stiffness matrix $K_{\Delta T}(\Delta T)$ on the left-hand-side and as a thermal force vector $\boldsymbol{F}_{\Delta T}$ on the right-hand-side.

In the indirect stiffness evaluation approach, the equation of motion is written in the form

$$\boldsymbol{M}\ddot{\boldsymbol{X}}(t) + \boldsymbol{C}\dot{\boldsymbol{X}}(t) + \boldsymbol{F}_{NL}[\boldsymbol{X}(t), \Delta T] = \boldsymbol{F}(t) \tag{2}$$

Here, the thermal effect is represented entirely on the left-hand-side of the equation in the nonlinear restoring force $\boldsymbol{F}_{\mathrm{NL}}$, which also contains the linear, quadratic, and cubic stiffness terms. Comparing Eqs. (1) and (2), a relationship between direct and indirect formulations is established, namely,

$$\boldsymbol{F}_{NL}[\boldsymbol{X}(t), \Delta T] = \{K_L - K_{\Delta T}(\Delta T) + K_1[\boldsymbol{X}(t)] + K_2[\boldsymbol{X}(t), \boldsymbol{X}(t)]\}\boldsymbol{X}(t) - \boldsymbol{F}_{\Delta T} \tag{3}$$

Continuing with the indirect approach, a set of coupled modal equations with reduced DOF is obtained by applying the modal coordinate transformation $\boldsymbol{X} = \boldsymbol{\Phi}\boldsymbol{q}$ to Eq. (2), in which $\boldsymbol{q}$ is the modal displacement response vector. In this study, the set of modal basis functions $\boldsymbol{\Phi}$ is formed from the linear eigenvalue problem without the effect of temperature. These are sometimes referred to as "cold modes." Generally, a small set of L basis functions is included, resulting in a modal equation of motion that takes the form

$$\tilde{\boldsymbol{M}}\ddot{\boldsymbol{q}}(t) + \tilde{\boldsymbol{C}}\dot{\boldsymbol{q}}(t) + \tilde{\boldsymbol{F}}_{NL}[q_1(t), q_2(t), \ldots, q_L(t), \Delta T] = \tilde{\boldsymbol{F}}(t) \tag{4}$$

The tilde superscript represents modal quantities, and

$$\tilde{\boldsymbol{M}} = \boldsymbol{\Phi}^T\boldsymbol{M}\boldsymbol{\Phi} = \lceil \boldsymbol{I} \rfloor, \qquad \tilde{\boldsymbol{C}} = \boldsymbol{\Phi}^T\boldsymbol{C}\boldsymbol{\Phi} = \lceil 2\zeta_r\omega_r \rfloor$$
$$\tilde{\boldsymbol{F}}_{\mathrm{NL}} = \boldsymbol{\Phi}^T\boldsymbol{F}_{\mathrm{NL}}, \qquad \tilde{\boldsymbol{F}} = \boldsymbol{\Phi}^T\boldsymbol{F} \tag{5}$$

B. Indirect Stiffness Evaluation Method

The previously developed [15,17] indirect stiffness evaluation procedure is used. To summarize, the rth element of the nonlinear restoring force vector in Eq. (4) can be formed by computing

$$\tilde{F}^r_{\mathrm{NL}}(q_1, q_2, \ldots, q_L, \Delta T) = \sum_{j=1}^{L} d^r_j(\Delta T)q_j + \sum_{j=1}^{L}\sum_{k=j}^{L} a^r_{jk}q_jq_k + \sum_{j=1}^{L}\sum_{k=j}^{L}\sum_{l=k}^{L} b^r_{jkl}q_jq_kq_l \qquad r = 1, 2, \ldots, L \tag{6}$$

where d, a, and b are the linear, quadratic nonlinear, and cubic nonlinear modal stiffness coefficients, respectively. The indirect stiffness evaluation procedure reduces the problem of determining the nonlinear modal stiffness to a series of static nonlinear problems with prescribed displacement fields and, if required, temperatures. The prescribed displacement fields are formed from combinations of modes in the basis. Once the resulting nonlinear forces are determined, the nonlinear modal stiffness coefficients may be found by solution of a simple algebraic system of equations. Note that the thermal loading can have an arbitrary spatial and through-the-thickness distribution, as long as such a distribution is supported by a commercial FE code used to compute the nonlinear restoring forces.

C. Implementation

The program RANSTEP was used to perform the reduced-order analysis with the indirect stiffness evaluation procedure. In particular, the RANSTEP implementation for MSC.NASTRAN was used because of successful application to similar problems [17]. The implementation consists of several steps. The linear eigenvectors are first obtained from a normal modes analysis (solution 103). The required displacement fields are then formed as a summation of selected and appropriately scaled basis functions. Next, a series of static nonlinear solutions (solution 106) are performed *at a prescribed elevated temperature* to obtain the corresponding restoring forces. Based on these forces, the modal stiffness coefficients are evaluated. The resulting coupled system of equations (4) is numerically integrated using the fourth-order Runge–Kutta scheme to obtain a modal displacement time history. An inverse modal transformation allows the physical displacement to be computed.

D. Finite Element Model

The beam under analysis measured $18 \times 1 \times 0.09$ in. (length by width by thickness). The FE model consisted of 144 CBEAM elements, each measuring 0.125 in. in length. Clamped boundary conditions were applied at both ends of the beam by specifying zero displacement and rotation. The following material properties were used:

$$E = 10.6 \times 10^6 \text{ psi}, \qquad G = 4.0 \times 10^6 \text{ psi}$$
$$\rho = 2.588 \times 10^{-4} \ \frac{\text{lb}_f - \text{s}^2}{\text{in.}^4}, \qquad \alpha = 12.4 \ \frac{\mu\text{-in./in.}}{^\circ F}$$

In the analyses that follow, mass proportional damping corresponding to critical damping of 2.0% for the fundamental mode (at 57.8 Hz) was specified.

Displacement results presented later in the paper are in the global coordinate system, which has its origin at the left clamped end of the beam. The x axis coincides with the beam midsurface and stretches along its span, with the positive y axis pointing upward. Thus, the in-plane u displacement is in the direction of the x axis, and the transverse v component is in the direction of the y axis.

E. Modal Basis Classification and Selection

It is helpful to categorize the linear eigenvectors that constitute the modal basis by their spatial distribution and by the dominant DOF

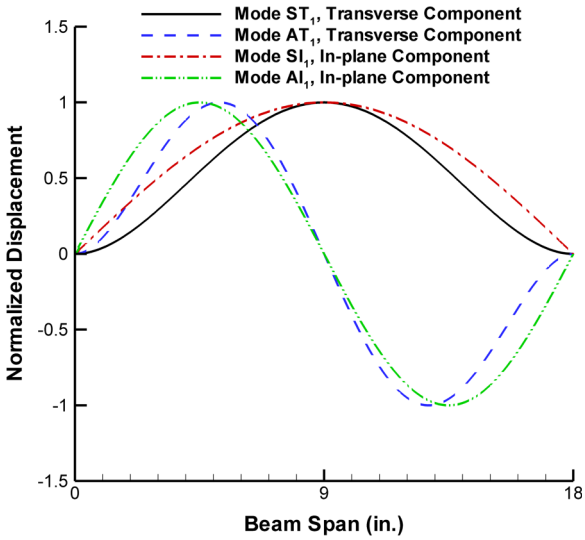

Fig. 1 Lowest ST, AT, SI and AI modes of clamped beam.

(e.g., transverse displacement). For the flat, isotropic, and symmetric beam structures considered herein, four categories are defined. Those having symmetric transverse displacements are subsequently referred to as symmetric transverse (ST) modes, and those having antisymmetric transverse displacements are referred to as antisymmetric transverse (AT) modes. Additionally, those having symmetric in-plane displacements are referred to as symmetric in-plane (SI) modes, and those having antisymmetric in-plane displacements are referred to as antisymmetric in-plane (AI) modes. Because of the absence of linear coupling between transverse and in-plane modes for the structure considered, both ST and AT modes have numerically zero in-plane displacement components u. Similarly, both SI and AI modes have numerically zero transverse displacement components v. Nonzero rotational DOF ϕ are present only in the transverse ST and AT modes. ST modes have an antisymmetric rotation distribution along the beam span, and AT modes have a symmetric rotation distribution along the beam span. The lowest mode of each of the four categories discussed earlier is presented in Fig. 1. The listing of the first six modes of each category is provided in Table 1. It is seen that the transverse ST and AT modes have lower natural frequencies than the in-plane SI and AI modes.

Table 1 Classification of selected eigenvectors

Mode designator	Mode number	Frequency, Hz
ST_1	1	57.78
ST_2	3	312.1
ST_3	7	770.1
ST_4	10	1430.6
ST_5	14	2292.5
ST_6	19	3354.3
AI_1	46	11,243
AI_2	81	22,480
AI_3	115	33,706
AI_4	153	44,917
AI_5	221	56,106
AI_6	231	67,268
AT_1	2	159.2
AT_2	4	515.7
AT_3	8	1075.1
AT_4	13	1836.5
AT_5	16	2798.5
AT_6	21	3959.7
SI_1	28	5621.5
SI_2	64	16,802
SI_3	98	28,095
SI_4	133	39,314
SI_5	178	50,514
SI_6	227	61,691

The most critical task in the reduced-order analysis is the selection of the modal basis, because it dictates the accuracy of the reduced-order solution. It may be intuitive to select a modal basis using characteristics of structural and loading symmetry. For example, for a symmetric planar structure under symmetric transverse loading, a modal basis consisting of only ST modes may suffice. Although such intuition may be useful for a linear analysis, it has been demonstrated for both flat [17] and curved [18] structures that such a rationale will lead to an inadequate basis selection for the nonlinear problem. This is due to coupling in the quadratic and cubic stiffness terms. Therefore, some additional guidance in the form of experimental data, theoretical or numerical analysis, or past reduced-order modeling experience is beneficial.

For the beam considered, several factors affected the modal basis selection used in this study. The first factor was earlier experience gained from a reduced-order analysis of symmetric planar structures under symmetric transverse loadings at room temperature ($\Delta T = 0$) conditions [17]. In this case, a combination of low-frequency ST modes and high-frequency AI modes was found to compare very well with a numerical simulation in physical DOF. From the study of shallowly curved structures [18], the additional inclusion of AT and SI modes was required to capture the in-plane behavior associated with autoparametric resonance. The geometry of the curved structure is similar to that of the thermally postbuckled beam, and hence the inclusion of AT and SI modes for the present problem is likely beneficial. Furthermore, during snap-through events, the transverse full-field displacements obtained from numerical simulation in physical DOF showed a nonsymmetric distribution (see Sec. III.B), indicating the participation of both ST and AT modes. Additionally, significant in-plane motion of the center node from the physical DOF analysis (see Sec. III.B) was found to accompany the snap-through response, further substantiating the need for SI modes in the modal basis. Thus, the modal basis chosen for this study consisted of all four types of modes. The six lowest modes of each four types were used to establish the modal basis. In the discussion that follows, this set will be referred to as the 24-mode basis.

To explore the impact of selecting an insufficient basis on the quality of the reduced-order results, a truncated basis was assembled from the six lowest ST modes and the six lowest AI modes. This basis was successfully previously applied for unbuckled structures [17]. In the present study, however, it lacks the SI modes necessary to capture the in-plane motion at the beam center and the AT modes necessary to capture the antisymmetric part of the transverse response, both of which participate in snap-through events. In the following, it will be referred to as the 12-mode basis.

Although developing a general and reliable methodology for optimal basis selection is of interest, such a task exceeds the scope of this work. A new rigorous modal-basis-selection procedure using proper orthogonal decomposition (POD) [19,20] analysis is presently under development [21].

F. Modal Stiffness Coefficients

The behavior of modal stiffness coefficients as a function of applied temperature increment was examined and warrants a discussion. For the purpose of this investigation, modal stiffness coefficients were computed at room temperature and at two uniformly distributed temperature increments of 35 and 70°F. There was no thermal gradient through the thickness. Because the critical buckling temperature ΔT_{CR} of the beam was found to be 6.6°F, the two elevated-temperature cases corresponded to approximately 5.3 and 10.6 times ΔT_{CR}, respectively.

Examination of the nonlinear quadratic and cubic modal stiffness matrices revealed that they were not affected by the temperature change. This observation is in agreement with the direct reduced-order FE formulation, in which the nonlinear stiffness matrices are only a function of displacement, regardless of how this displacement was induced [13,14]. The linear modal stiffness coefficients, however, were found to be strongly dependent on the temperature change. For the room temperature condition, the linear modal stiffness matrix is uncoupled. The linear stiffness coefficients are the

positive eigenvalues and equal to the square of the natural frequencies of the system. Further, because the matrix is diagonal, the linear modal stiffness does not contribute to the overall coupling of transverse and in-plane modes. At elevated temperatures, some of the off-diagonal stiffness terms become significant, resulting in a coupled linear modal stiffness matrix. For both temperatures and bases considered, only the portion of the linear matrix corresponding to the low-frequency transverse modes (ST in the 12-mode basis and ST and AT in the 24-mode basis) was altered. The off-diagonal terms were symmetric. These observations are also consistent with the previous direct reduced-order FE development [13,14]. Moreover, in the case of the 12-mode basis, the low-frequency portion of the linear stiffness was fully populated, effectively coupling all ST modes included in the basis. In the case of the 24-mode basis, the coupling between ST modes was large, and the coupling between AT modes was large, but no linear cross-coupling occurred between the ST and AT modes. These observations are illustrated in Tables 2–4, with excerpts from the linear modal stiffness matrices computed with the 24-mode basis at different thermal loadings.

Another observation from Tables 2–4 is that the linear stiffness coefficients vary linearly with temperature. Relative to the room temperature condition, the change in magnitude of a linear stiffness coefficient computed at a ΔT of 70°F is double that of the value computed at a ΔT of 35°F. Again, this observation is consistent with the direct reduced-order FE development and with previous indirect method work [15]. Although this observation is not needed in the process of computing the set of modal stiffness coefficients by the indirect stiffness evaluation method, it may be exploited when temporal temperature variations are required in the analysis. Effectively, it allows a significant computational savings, because only a few linear modal coefficients must be scaled, but not reevaluated, as the temperature changes.

Finally, for the elevated temperature case, the change in sign of the affected diagonal terms from positive to negative provides useful information. Consider a basis consisting of only the first ST mode, so that the linear stiffness corresponds to only the ST_1–ST_1 entry in Tables 2–4. A straight-line fit as a function of temperature indicates a change in sign at 6.8°F. Because the first ST mode greatly contributes to the first buckled shape, the temperature at which the sign changes is close to the first critical buckling temperature ΔT_{CR1} of 6.6°F. Similarly, a basis consisting of only the first AT mode shows a stiffness sign change at 13.9°F, which is close to the second critical buckling temperature ΔT_{CR2} of 13.6°F. As the temperature increases, the number of negative diagonal entries increases. For example, there are three negative diagonal entries in Table 3 for a ΔT of 35°F and four negative diagonal entries in Table 4 for a ΔT of 70°F.

Table 2 Selected modal linear stiffness d_{ij} coefficients ($\times 10^6$) for the 24-mode basis at $\Delta T = 0$°F

	ST_1	AT_1	ST_2	AT_2
ST_1	0.132	0	0	0
AT_1	sym	1.001	0	0
ST_2	sym	sym	3.845	0
AT_2	sym	sym	sym	10.50

Table 3 Selected modal linear stiffness d_{ij} coefficients ($\times 10^6$) for the 24-mode basis at $\Delta T = 35$°F; bold entries indicate cross-coupling between the modes

	ST_1	AT_1	ST_2	AT_2
ST_1	−0.543	0	**0.534**	0
AT_1	sym	−1.524	0	**−0.940**
ST_2	sym	sym	−1.577	0
AT_2	sym	sym	sym	1.098

Table 4 Selected modal linear stiffness d_{ij} coefficients ($\times 10^6$) for the 24-mode basis at $\Delta T = 70$°F; bold entries indicate cross-coupling between the modes

	ST_1	AT_1	ST_2	AT_2
ST_1	−1.218	0	**1.068**	0
AT_1	sym	−4.049	0	**−1.880**
ST_2	sym	sym	−6.998	0
AT_2	sym	sym	sym	−8.303

III. Dynamic Thermal-Buckling Analysis

The dynamic response during thermal buckling is of interest because it captures the characteristics of a single snap-through event. The dynamic thermal-buckling event was induced by an instantaneous temperature increase of 35°F, uniformly distributed along the length of the beam with a zero through-the-thickness gradient. The beam was initially at rest, with zero displacement and velocity. In the case of the reduced-order analysis, the initial conditions were specified in modal coordinates. A small decaying transverse perturbation force having an initial magnitude of 0.125 lbf was applied at the midspan node to trigger the stability loss. The force linearly decayed to zero over the period of 0.5 s. A fixed integration time step of 1 μs was used for all reduced-order analyses.

A. Physical DOF Analysis

For comparison purposes, the physical DOF analysis was performed using ABAQUS/Explicit. The double-precision explicit integration scheme with an automatically determined stable integration time step (referred to as "element by element" in ABAQUS) was used for all analyses. The finite element model used was identical to the MSC.NASTRAN-based model used in the RANSTEP reduced-order analysis, except that ABAQUS B21 beam elements were used in place of CBEAM elements. Previous work [17] demonstrated that good comparisons can be achieved between a reduced-order analysis using MSC.NASTRAN and physical simulation using ABAQUS/Explicit.

B. Thermal-Buckling Response

The displacement response of the quarter-span and the midspan nodes is shown in Figs. 2 and 3 for the transverse and in-plane

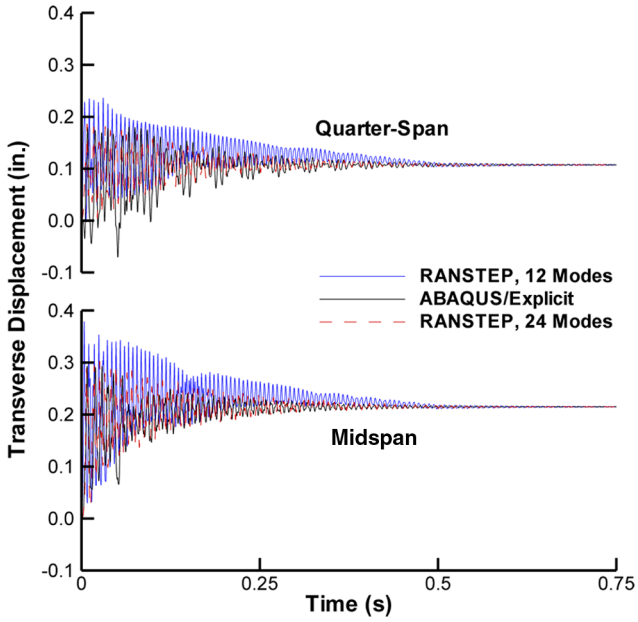

Fig. 2 Transverse displacement response of a dynamic thermal-buckling event.

components, respectively. At the midspan location, only the ST modes directly contribute to the transverse response, because the AT modes have a node at this location. Similarly, only the SI modes directly contribute to the in-plane response at the midspan location, because the AI modes have a node there. The effect of the AT and AI modes at the midspan is therefore manifested indirectly by altering the system of modal equations. Consequently, modal time histories corresponding to modes ST and AI differ between the 12- and 24-mode bases.

In Fig. 2, the 24-mode RANSTEP and physical DOF analyses agree quite well, rising from the zero condition with a damped transient response about the final buckling displacement of 0.215 in. for the midspan location. The 12-mode RANSTEP analysis comes to the same final displacement, but oscillates more toward the positive side of the final displacement. In Fig. 3, it is interesting to note that significant in-plane response at the midspan location is not instantaneous, but is delayed by about 0.05 s, clearly indicating the time-varying contribution of the SI modes. Because the 12-mode basis lacked the SI modes, this basis was incapable of representing any in-plane behavior at the midspan location. This establishes the importance of including the SI modes in the solution. At the quarter-span location, the in-plane transient response characteristic is captured more accurately by the 24-mode basis than by the 12-mode basis, which displays oscillations more toward the negative side of the final displacement. At both locations, the damped transient response eventually settles to the zero in-plane displacement associated with the static buckled shape.

Presented in Fig. 4 is the difference between the transverse displacements computed at the quarter-span and three-quarter-span locations (i.e., responses at the nodes located 4.5 in from the clamped ends). Because the difference computed by numerical simulation in physical DOF has nonzero values in the transient period of the response, it is concluded that the transverse displacement response is nonsymmetric during the thermal-buckling event. Consequently, for a successful modal reduction, the basis must be composed of both symmetric and antisymmetric transverse modes (i.e., ST and AT modes). The result obtained with the 24-mode basis exhibits a very similar characteristic to the one obtained with numerical simulation in physical DOF, whereas the 12-mode basis is incapable of capturing this effect because it lacks AT modes. This establishes the necessity of also including AT modes in the solution.

Note that a static postbuckling analysis performed with MSC.NASTRAN solution 106 (not shown) yielded nearly identical

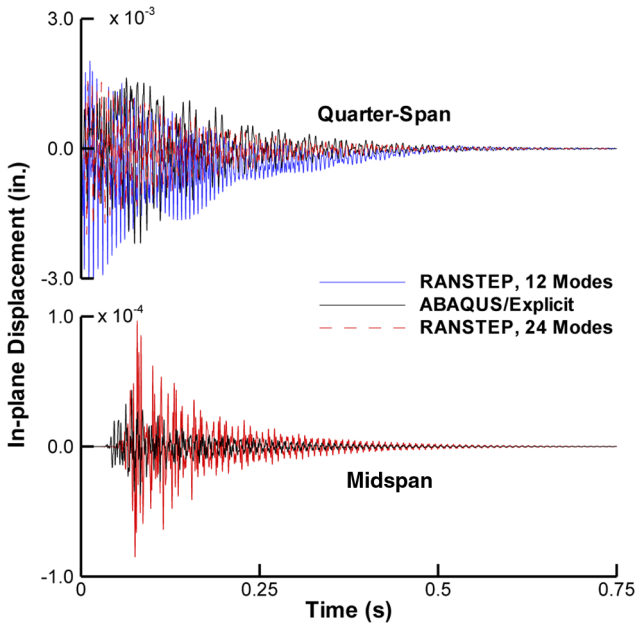

Fig. 3 In-plane displacement response of a dynamic thermal-buckling event.

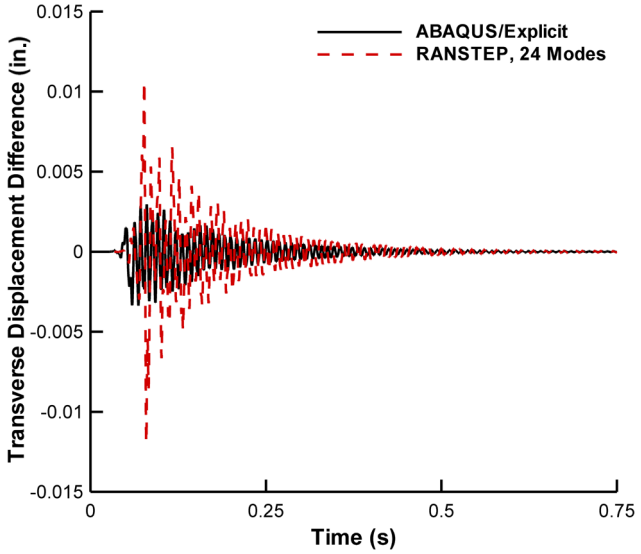

Fig. 4 Transverse displacement response difference of a dynamic thermal-buckling event.

final buckling displacements. Hence, there are insignificant differences in the manner in which the thermal loading is handled between the NASTRAN-based RANSTEP analysis and the ABAQUS analysis. What is important about the dynamic thermal bucking analysis in this work, however, is not the final at-rest state, but the transient response leading to that state. In this light, the 24-mode basis best captures the relevant dynamics of the single snap-through event. The thermal-acoustic response considered next consists of multiple snap-through events. Therefore, it is expected that the 24-mode basis will also better represent the dynamics than the 12-mode basis.

IV. Thermal-Acoustic Response Analysis

The dynamic response of the beam to a combined thermal-acoustic load was next investigated. The thermal load was instantaneously applied to the beam via a uniformly distributed temperature increase of 35°F with a zero through-the-thickness gradient. A Gaussian random pressure load with a flat excitation spectrum from 0–1500 Hz was generated using a previously developed procedure [22]. The frequency range of the pressure loading was lower than the maximum frequency of the low-frequency ST and AT modes. Almost half of those selected were outside the excitation bandwidth, whereas all of the SI and AI modes resided significantly above the excitation bandwidth. The pressure was uniformly applied along the span in the transverse direction, irrespective of the deformation (i.e., follower forces were not used). Excitation levels of 128, 158, and 170 dB were considered so that different response regimes could be investigated.

The beam was initially at rest, with zero displacement and velocity, in the unbuckled state. A simulated response time history of 2.1384 s was performed at each level considered. In the computation of power spectral density (PSD) and probability density function (PDF), five ensembles were averaged. For each ensemble, the initial 0.5 s was removed to eliminate the startup transient. In the case of Poincaré maps, only a single ensemble with the initial 0.5 s removed was used for a better clarity of plots. Also, only a single ensemble was used to compute the Lyapunov exponents, the computation of which was based on the algorithm offered by Wolf et al. [23].

A. Thermal-Acoustic Response

The three response regimes are illustrated with ABAQUS/Explicit-generated transverse displacement time histories of the midspan node in Fig. 5. The regimes can be characterized as 1) small-amplitude vibration around one of the two stable buckled equilibrium positions (128 dB), 2) intermittent snap-through response between the two buckling equilibrium positions (158 dB), and 3) persistent

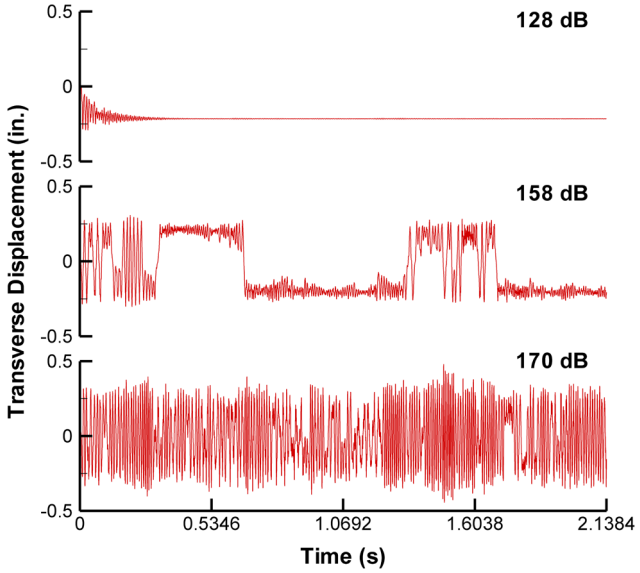

Fig. 5 Transverse displacement response at 35°F and 128, 158, and 170 dB excitations.

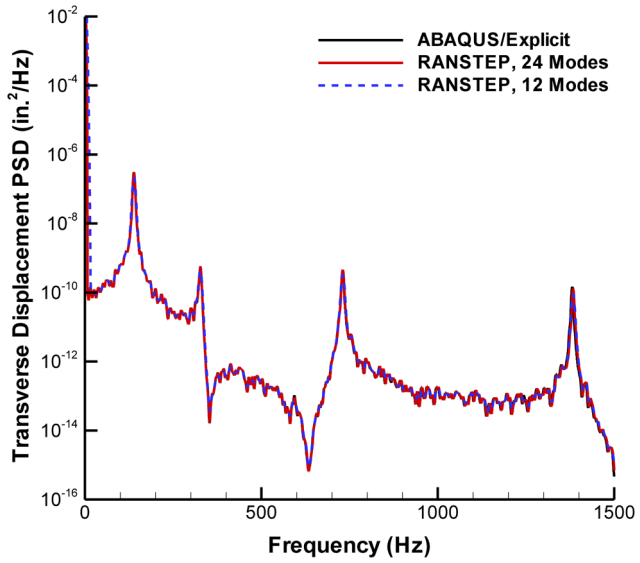

Fig. 6 Midspan transverse displacement response PSD at 35°F and 128 dB.

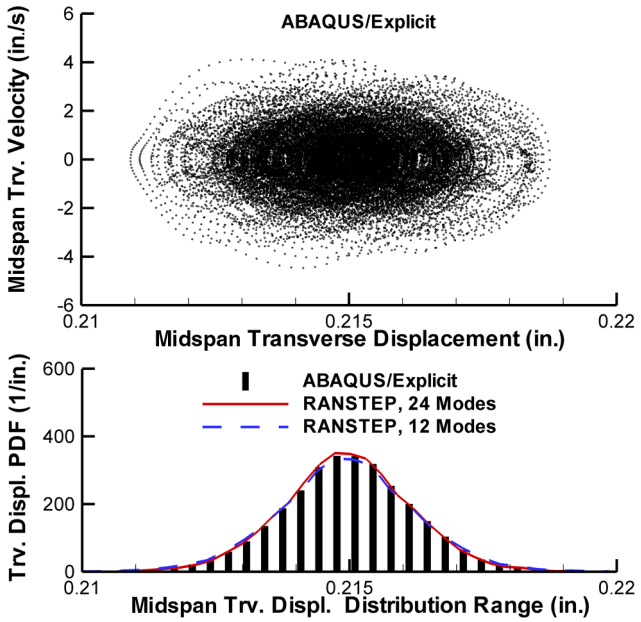

Fig. 7 Transverse displacement Poincaré map and PDF at 35°F and 128 dB.

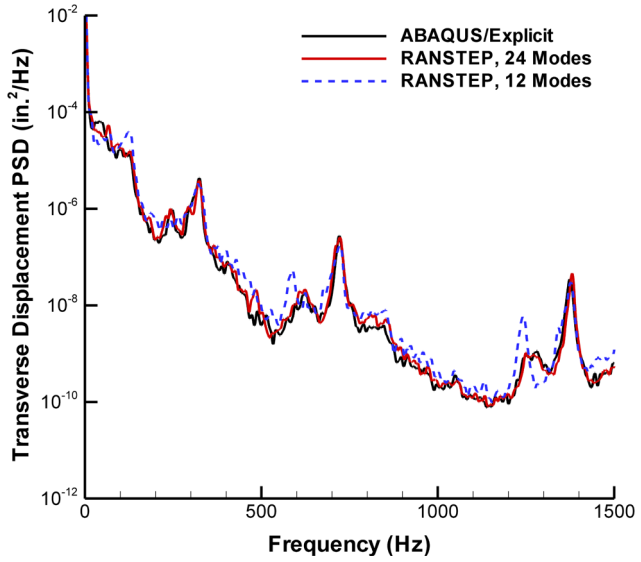

Fig. 8 Midspan transverse displacement response PSD at 35°F and 158 dB.

snap-through response between the two equilibrium positions (170 dB).

The PSD of the midspan transverse displacement response at 128 dB is shown in Fig. 6. Because the time histories from which these were generated lacked the initial thermal-buckling transient, the results from the 12- and 24-mode bases compare equally well with the physical DOF simulation. A significant static displacement component due to thermal buckling is apparent. The corresponding Poincaré map and the PDF exhibiting a Gaussian distribution with a nonzero mean are shown in Fig. 7. With the initial thermal-buckling transient removed, the in-plane displacement response was negligible at this location. The Lyapunov exponent computed for this case converged to a negative value, indicating that a chaotic response was not induced.

When the excitation level is increased such that intermittent snap-through response occurs, differences between the 12- and 24-mode bases become apparent. Figure 8 shows the PSD of the midspan transverse displacement response at 158 dB. Very good agreement is noted between the 24-mode and physical DOF analyses across the frequency range. The 12-mode reduced-order analysis, however, exhibits amplification at some peaks. All three analyses reflect the dominant zero-frequency component. The in-plane response is shown in Fig. 9. Again, the 24-mode solution captured all of the essential features of the physical response. The 12-mode solution is unable to produce any in-plane displacement response, due to the lack of SI modes in the basis.

The transverse displacement Poincaré map and the PDF at the midspan are shown in Fig. 10. Based on these two representations, it is clear that the majority of vibration cycles at this level occurred about either of the two thermally buckled equilibrium positions. In particular, for the simulation period considered, the structure happened to spend more time oscillating about the lower equilibrium position. This is also consistent with the 158-dB time-history response presented in Fig. 5. Small values of the probability density in the proximity of the zero-distribution range (Fig. 10) indicate the few instances when the response snapped between the two equilibrium positions. The Lyapunov exponent computed for the midspan transverse displacement showed a positive value, indicative of chaotic motion. Because of intermittent snap-thorough, however, its temporal convergence was not achieved.

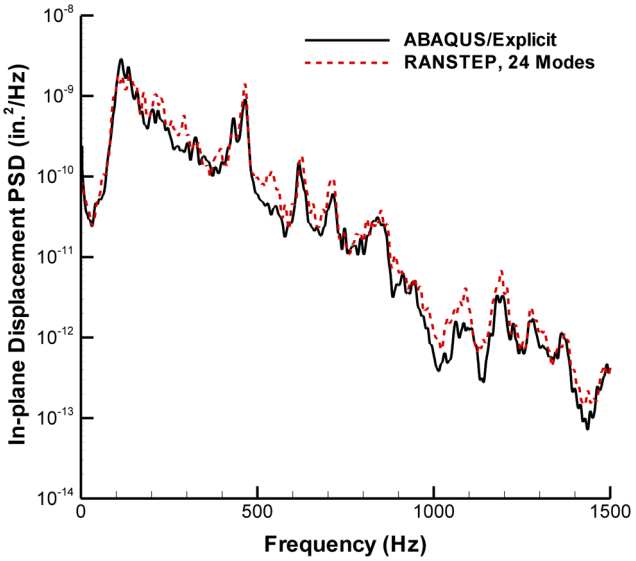

Fig. 9 Midspan in-plane displacement response PSD at 35°F and 158 dB.

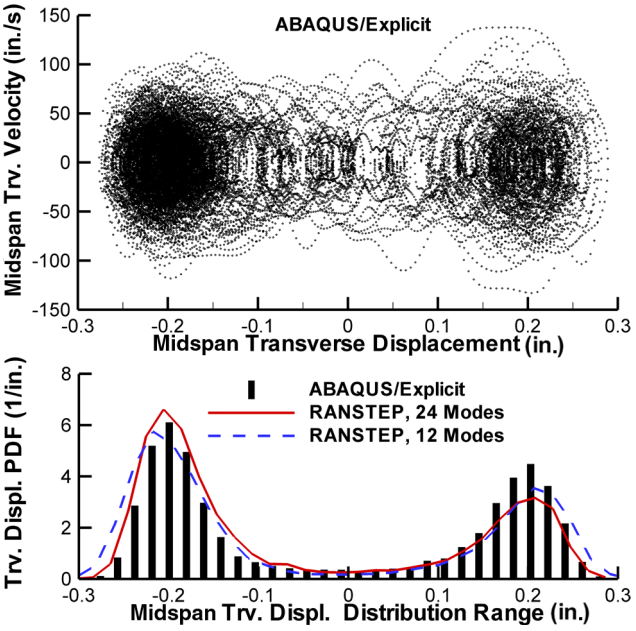

Fig. 10 Transverse displacement Poincaré map and PDF at 35°F and 158 dB.

It is often advantageous to observe the behavior at more than one location on the structure to help further identify liabilities and limitations associated with modal reduction. The quarter-span location was selected for this purpose, because the dynamic displacement response there exhibits significant in-plane and transverse components. The quarter-span transverse displacement response PSD at the 158-dB excitation level is shown in Fig. 11. Like the midspan response in Fig. 8, the 24-mode solution compares favorably with the physical DOF solution across the frequency range. Above 1 kHz, the 12-mode solution misses one peak and amplifies another. Again, the dominant zero-frequency component is seen. The quarter-span in-plane displacement PSD is shown in Fig. 12. The 24-mode solution again compares favorably with the physical DOF solution across the frequency range, whereas the 12-mode solution poorly matches the physical response in the low- and high-frequency ranges.

To help better understand how these differences manifest themselves and what their origins are, one can observe the contribution of various modal displacement components. Plotted in

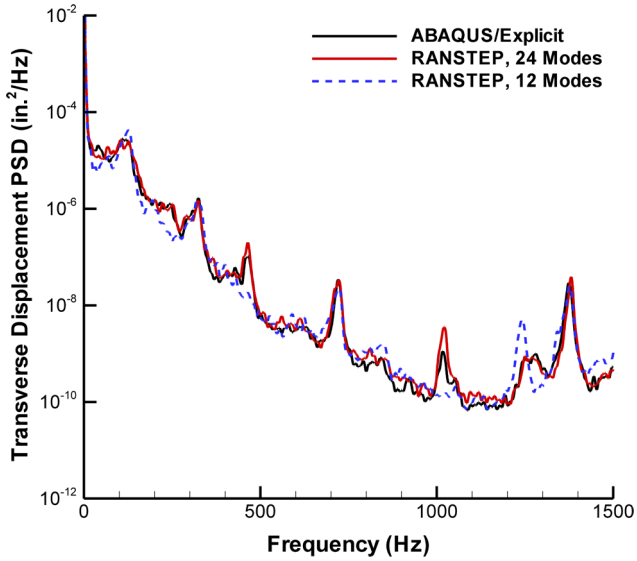

Fig. 11 Quarter-span transverse displacement response PSD at 35°F and 158 dB.

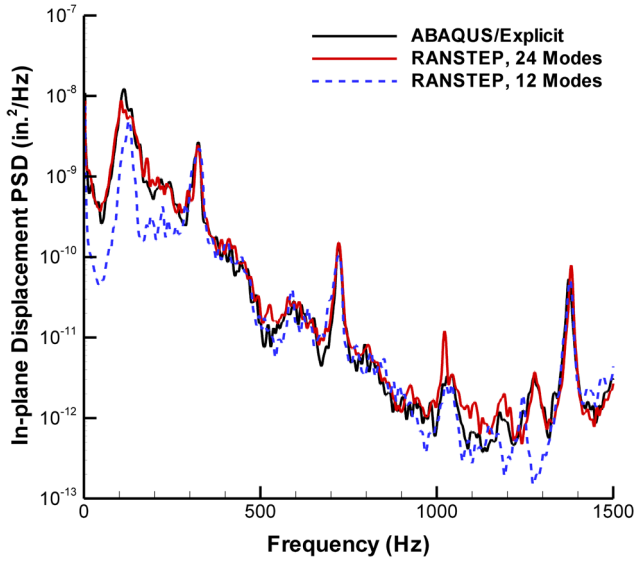

Fig. 12 Quarter-span in-plane displacement response PSD at 35°F and 158 dB.

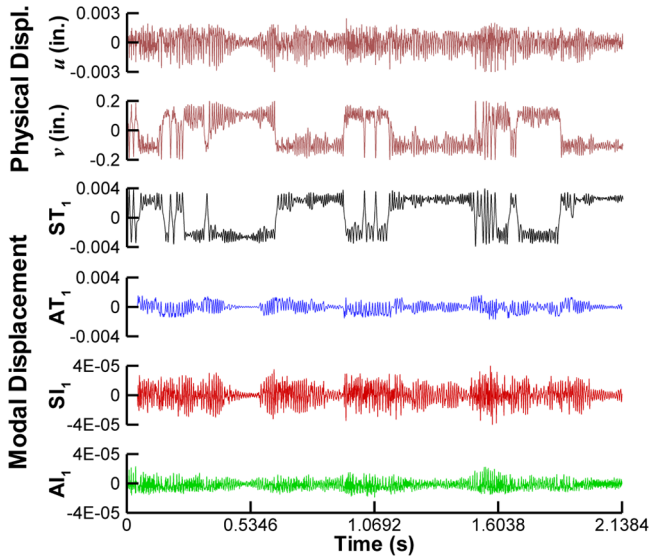

Fig. 13 Quarter-span physical and modal displacement response at 35°F and 158 dB.

Fig. 13 are the lowest components of each mode type (ST_1, AT_1, SI_1, and AI_1) for the 24-mode reduced-order solution at 35°F and 158 dB. Also plotted are the reduced-order in-plane and transverse displacement time histories obtained from the inverse modal transformation at the quarter-span location. The modal responses from modes ST_1 and AT_1 are on the order of 10^{-3}, whereas those from the SI_1 and AI_1 modes are two orders of magnitude smaller. Note, however, that the magnitude of the modal response is not indicative of its contribution to the physical response, because the latter is a superposition of all modal contributors through the inverse coordinate transformation and is location-specific. Mode ST_1 is strongly correlated with the transverse physical displacement v. The correlation coefficient has a value of −0.92. Similarly, mode AI_1 is strongly correlated with the in-plane physical displacement u, with the correlation coefficient of −0.83. For both correlation coefficients, the negative signs originate from a normalization of the ST_1 and the AI_1 eigenvector to a negative value.

Of most interest in Fig. 13 are modes SI_1 and AT_1, which are not included in the 12-mode basis. These modes exhibit similar behavior to that of the decaying in-plane transient response of the single dynamic thermal-buckling event, first seen in Fig. 3. Unlike the midspan location, both modes directly contribute to the response at the quarter-span location. A significant increase in the SI_1 and AT_1 modal responses occurs at every snap-through event. Hence, these modes play an important role in the response during such events and further indicate that the 12-mode basis is insufficient for accurately capturing the snap-through response.

The midspan transverse and in-plane displacement response PSDs, obtained at a ΔT of 35°F and at the 170 dB excitation level, are presented in Figs. 14 and 15, respectively. This excitation level was shown in Fig. 5 to result in a persistent snap-through response. Both 24-mode PSDs compare very well with the physical DOF solution. As expected, the transverse response PSD from the 12-mode solution compares less favorably and does not exist for the in-plane response. Because of the persistent snap-through response, the transverse static component was no longer dominant, as shown in Fig. 14. The transverse displacement Poincaré map and PDF for this loading condition are shown in Fig. 16. Here it is shown that as the intensity of snap-through is increased, the rate of the zero-crossings increases. Hence, the center part of the PDF distribution fills in compared with the intermittent snap-through conditions. The PDF obtained with the 24-mode basis matches the PDF distribution obtained from the physical DOF analysis better than with the 12-mode solution. The 12-mode solution reveals too broad a distribution range and generally tends to underestimate the probability density. The

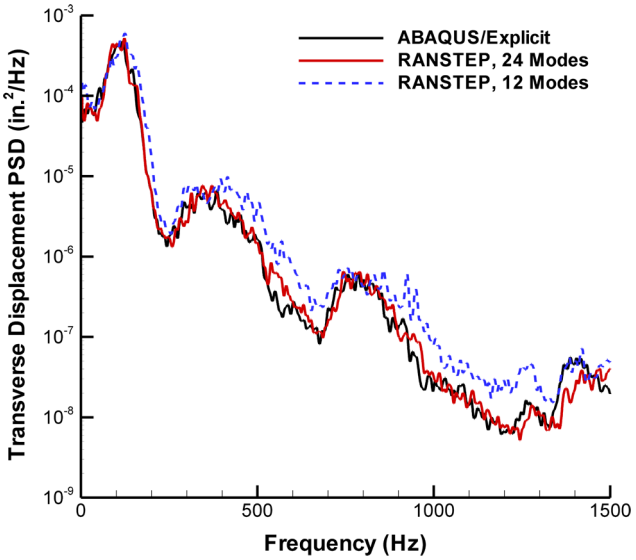

Fig. 14 Midspan transverse displacement response PSD response at 35°F and 170 dB.

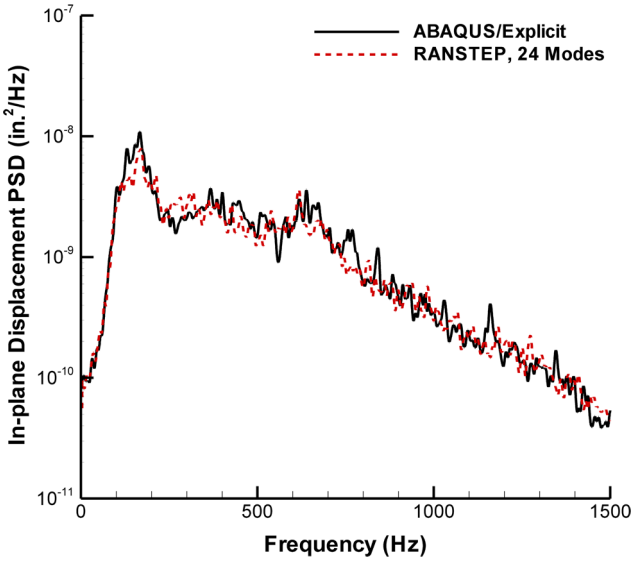

Fig. 15 Midspan in-plane displacement response PSD at 35F and 170 dB.

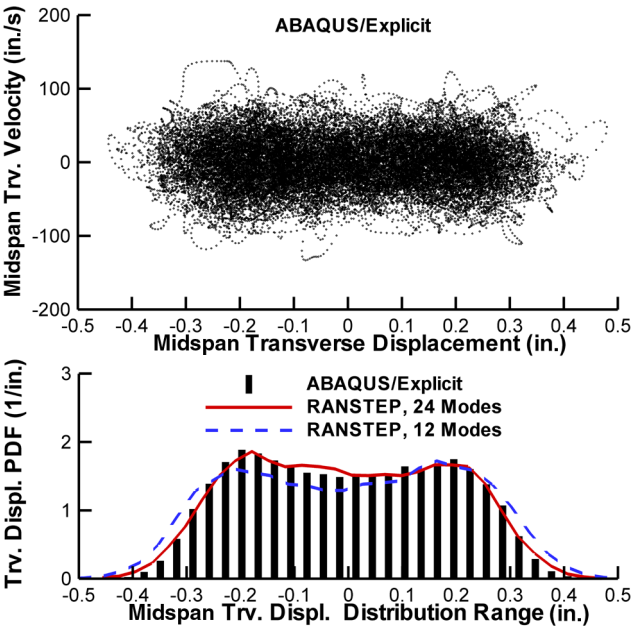

Fig. 16 Midspan transverse displacement Poincaré map and PDF at 35F and 170 dB.

Lyapunov exponent computed at this excitation level was positive, and a good temporal convergence was achieved. Consequently, the response can be regarded as being chaotic.

Finally, for a fixed temperature increment of 35°F, the number of transverse displacement zero-crossings is presented as a function of the random-pressure-excitation level. Having good agreement in the number of crossings is of interest, because large excursions associated with snap-through will significantly influence the fatigue life.

It is seen in Fig. 17 that snap-through does not occur up to a random pressure level of about 152 dB (0.1152 psi). Then, beginning in the range between 152 and 158 dB (0.2304 psi), the snap-through behavior is initiated and the number of zero-crossings starts growing as the excitation level is further increased. Results obtained in physical DOF and by the reduced-order analysis using 24-mode reduction are in a good agreement, despite the relatively short simulation time studied. Thus, the suitability of the reduced-order analysis for subsequent fatigue studies is further established.

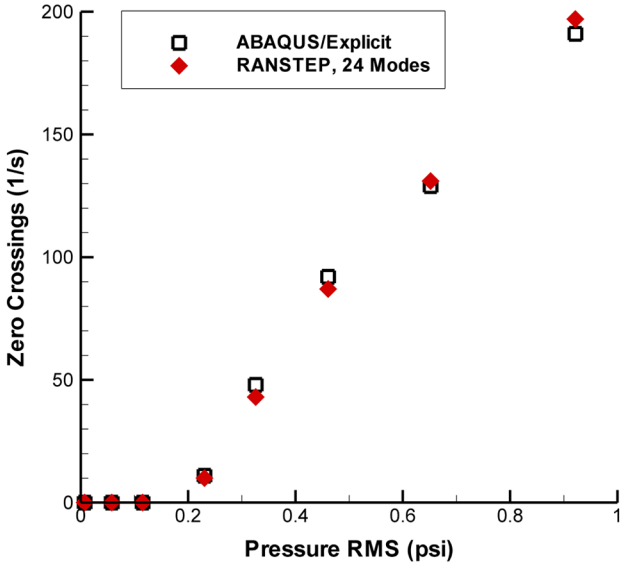

Fig. 17 Transverse displacement zero-crossing intensity at 35F.

V. Conclusions

A reduced-order FE-based method for predicting thermoacoustic random response in a nonlinear regime was presented. Two sets of modal bases were examined in the study, and the corresponding reduced-order analysis results were compared with solutions obtained with an analysis in physical DOF.

The effect of elevated temperature on the modal stiffness coefficients was first examined. It was found that only the linear stiffness coefficients corresponding to low-frequency transverse displacement modes were affected by the temperature change. These stiffness coefficients were found to vary linearly with temperature. Quadratic and cubic stiffness coefficients were unaffected. As a result, a computational benefit may be gained for problems with a time-varying thermal loading magnitude, because linear coefficients need only be scaled.

In the analysis of dynamic thermal-buckling and thermal-acoustic responses, it was found that a modal basis consisting of four types of modes (ST, AT, SI, and AI) more accurately predicted the response than a basis consisting of only ST and AI modes. In particular, for both loading conditions, the contribution of SI and AT modes becomes more significant as the structure transitions to a different equilibrium position.

Although not in scope of this study, the fatigue life will be affected in a different manner depending on the response regime. For the response about one of the thermally buckled equilibrium positions, a significant tensile mean stress component will be introduced on one side of the beam. The tensile mean stress has been shown to adversely affect the fatigue life [24–26]. Additionally, for intermittent and persistent snap-through, large cyclic stress amplitudes will rapidly accumulate and lead to a shorter fatigue life. Therefore, a continuation of this study to address stress recovery and fatigue estimation is deemed to be worthwhile.

References

[1] Pozefsky, P., Blevins, R. D., and Langanelli, A. L., "Thermal-Vibro-Acoustic Loads and Fatigue of Hypersonic Flight Vehicle Structure," Wright Labs., Rept. AFWAL-TR-89-3014, Wright–Patterson AFB, OH, 1989.

[2] Istenes, R. R., Rizzi, S. A., and Wolfe, H. F., "Experimental nonlinear random vibration results of thermally buckled composite panels," *36th AIAA/ASME/ASCE/AHS/ASC Structures, Structural Dynamics and Materials Conference*, AIAA, Washington, DC, 1995, pp. 1559–1568; also AIAA Paper 95-1345-CP.

[3] Murphy, K. D., Virgin, L. N., and Rizzi, S. A., "Experimental Snap-Through Boundaries for Acoustically Excited, Thermally Buckled Plates," *Experimental Mechanics*, Vol. 36, No. 4, 1996, pp. 312–317.

[4] Ng, C. F., and Clevenson, S. A., "High-Intensity Acoustic Tests of a Thermally Stressed Plate," *Journal of Aircraft*, Vol. 28, No. 4, 1991, pp. 275–281.

[5] Lee, J., "Displacement and Strain Histograms of Thermally Buckled Composite Plates in Random Vibration," 37th AIAA/ASME/ASCE/AHS/ASC Structures, Structural Dynamics, and Materials Conference, Salt Lake City, UT, AIAA Paper 96-1347, 1996.

[6] Lee, J., "Displacement and Strain Statistics of Thermally Buckled Plates," *Journal of Aircraft*, Vol. 38, No. 1, 2001, pp. 104–110.

[7] Lee, J., Vaicaitis, R., Wentz, K., Clay, C., Anselmo, E., and Crumbacher, R., "Predicition of Statistical Dynamics of Thermally Buckled Composite Plates," 39th AIAA/ASME/ASCE/AHS/ASC Structures, Structural Dynamics, and Materials Conference, Long Beach, CA, AIAA Paper 98-1975, 1998.

[8] Ng, C. F., "Nonlinear and Snap-Through Response of Curved Panels to Intense Acoustic Excitation," *Journal of Aircraft*, Vol. 26, No. 3, 1989, pp. 281–288.

[9] Ng, C. F., and Wentz, K. R., "The Prediction and Measurement of Thermoelastic Response of Plate Structures," 31st AIAA/ASME/ASCE/AHS/ASC Structures, Structural Dynamics, and Materials Conferece, Long Beach, CA, AIAA Paper 1990-988, 1990.

[10] Ghazarian, N., and Locke, J., "Nonlinear Random Response of Antisymmetric Angle-Ply Laminates Under Thermal-Acoustic Loading," *Journal of Sound and Vibration*, Vol. 186, No. 2, 1995, pp. 291–309.

[11] Maekawa, S., "On the Sonic Fatigue Life Estimation of Skin Structures at Room and Elevated Temperatures," *Journal of Sound and Vibration*, Vol. 80, No. 1, 1982, pp. 41–59.

[12] Duan, B., Mei, C., and Ro, J. J., "Nonlinear Response of Thermal Protection System at Supersonic Speeds," 42nd AIAA/ASME/ASCE/AHS/ASC Structures, Structural Dynamics, and Materials Conference, Seattle, WA, AIAA Paper 2001-1659, 2001.

[13] Guo, X., Przekop, A., and Mei, C., "Nonlinear Random Response of Shallow Shells at Elevated Temperatures Using Finite Element Modal Method," 45th AIAA/ASME/ASCE/AHS/ASC Structures, Structural Dynamics and Materials Conference, Palm Springs, CA, AIAA Paper 2004-1558, 2004.

[14] Mei, C., Dhainaut, J. M., Duan, B., Spottswood, S. M., and Wolfe, H. F., "Nonlinear Random Response of Composite Panels in an Elevated Thermal Environment," U.S. Air Force Research Lab., Rept. AFRL-VA-WP-TR-2000-3049, Wright–Patterson AFB, OH, Oct. 2000.

[15] Mignolet, M. P., Radu, A. G., and Gao, X., "Validation of Reduced Order Modeling for the Prediction of the Response and Fatigue Life of Panels Subjected to Thermo-Acoustic Effects," *Structural Dynamics: Recent Advances* [CD-ROM], edited by M. J. Brennan, M. A. Ferman, B. A. T. Petersson, S. A. Rizzi, and K. Wentz, Inst. of Sound and Vibration Research, Univ. of Southampton, Southampton, England, U.K., 2003.

[16] Muravyov, A. A., and Rizzi, S. A., "Determination of Nonlinear Stiffness with Application to Random Vibration of Geometrically Nonlinear Structures," *Computers and Structures*, Vol. 81, No. 15, 2003, pp. 1513–1523.

[17] Rizzi, S. A., and Przekop, A., "The Effect of Basis Selection on Static and Random Acoustic Response Using a Nonlinear Modal Simulation," NASA Langley Research Center TP-2005-213943, Hampton, VA, Dec. 2005.

[18] Przekop, A., and Rizzi, S. A., "Nonlinear Reduced Order Finite Element Analysis of Structures with Shallow Curvature," *AIAA Journal*, Vol. 44, No. 8, 2006, pp. 1767–1778.

[19] Feeny, B. F., "On Proper Orthogonal Co-Ordinates as Indicators of Modal Activity," *Journal of Sound and Vibration*, Vol. 255, No. 5, 2002, pp. 805–817.

[20] Feeny, B. F., and Kappagantu, R., "On the Physical Interpretation of Proper Orthogonal Modes in Vibrations," *Journal of Sound and Vibration*, Vol. 211, No. 4, 1998, pp. 607–616.

[21] Rizzi, S. A., and Przekop, A., "POD/MAC-Based Modal Basis Selection for a Reduced Order Nonlinear Response Analysis," *EUROMECH 483: Geometrically Non-Linear Vibrations of Structures*, 483, Faculdade de Engenharia (FEUP), Univ. do Porto, Porto, Portugal, 2007, pp. 101–104.

[22] Rizzi, S. A., and Muravyov, A. A., "Comparison of Nonlinear Random Response Using Equivalent Linearization And Numerical Simulation," *Structural Dynamics: Recent Advances*, Vol. 2, edited by N. S. Ferguson, H. F. Wolfe, M. A. Ferman, and, S. A. Rizzi, Inst. of Sound and Vibration Research, Univ. of Southampton, Southampton, England, U.K., 2000, pp. 833–846.

[23] Wolf, A., Swift, J. B., Swinney, H. L., and Vastano, J. A., "Determining Lyapunov Exponents from a Time Series," *Physica D*, Vol. 16, No. 1985, pp. 285–317.

[24] Rizzi, S. A., and Przekop, A., "Estimation of Sonic Fatigue by Reduced-

Order Finite Element Based Analysis," *Structural Dynamics: Recent Advances*, edited by M. J. Brennan, B. R. Mace, J. M. Muggleton, S. Liguore, K. D. Murphy, B. A. T. Petersson, S. A. Rizzi, and R. Shen, Inst. of Sound and Vibration Research, Univ. of Southampton, Southampton, England, U.K., 2006.

[25] Sweitzer, K. A., and Ferguson, N. S., "Mean Stress Effects on Random Fatigue Analysis of Nonlinear Structures," *Twelfth International Congress on Sound and Vibration (ICSV12)* [CD-ROM], Technical Univ. of Lisbon, Lisbon, Portugal, 2006.

[26] Przekop, A., Rizzi, S. A., and Sweitzer, K. A., "An Investigation of High-Cycle Fatigue Models for Metallic Structures Exhibiting Snap-Through Response," 48th AIAA/ASME/ASCE/AHS/ASC Structures, Structural Dynamics, and Materials Conference, Honolulu, HI, AIAA Paper 2007-2204, 2007.

B. Balachandran
Associate Editor